scientific reports

Check for updates

OPEN

Organophosphorus diisopropylfluorophosphate (DFP) intoxication in zebrafish larvae causes behavioral defects, neuronal hyperexcitation and neuronal death

Alexandre Brenet[1,4], Julie Somkhit[1,4], Rahma Hassan-Abdi[1], Constantin Yanicostas[1], Christiane Romain[1], Olivier Bar[1], Alexandre Igert[2], Dominique Saurat[3], Nicolas Taudon[3], Gregory Dal-Bo[2], Florian Nachon[2], Nina Dupuis[2,5,5] & Nadia Soussi-Yanicostas[1,5,5]✉

With millions of intoxications each year and over 200,000 deaths, organophosphorus (OP) compounds are an important public health issue worldwide. OP poisoning induces cholinergic syndrome, with respiratory distress, hypertension, and neuron damage that may lead to epileptic seizures and permanent cognitive deficits. Existing countermeasures are lifesaving but do not prevent long-lasting neuronal comorbidities, emphasizing the urgent need for animal models to better understand OP neurotoxicity and identify novel antidotes. Here, using diisopropylfluorophosphate (DFP), a prototypic and moderately toxic OP, combined with zebrafish larvae, we first showed that DFP poisoning caused major acetylcholinesterase inhibition, resulting in paralysis and CNS neuron hyperactivation, as indicated by increased neuronal calcium transients and overexpression of the immediate early genes *fosab*, *junBa*, *npas4b*, and *atf3*. In addition to these epileptiform seizure-like events, DFP-exposed larvae showed increased neuronal apoptosis, which were both partially alleviated by diazepam treatment, suggesting a causal link between neuronal hyperexcitation and cell death. Last, DFP poisoning induced an altered balance of glutamatergic/GABAergic synaptic activity with increased NR2B-NMDA receptor accumulation combined with decreased GAD65/67 and gephyrin protein accumulation. The zebrafish DFP model presented here thus provides important novel insights into the pathophysiology of OP intoxication, making it a promising model to identify novel antidotes.

Organophosphorus (OP) compounds comprise highly poisonous substances widely used as chemical pesticides but also as warfare agents. As a result of their massive use for agricultural purposes worldwide, OP poisoning represents a major public health issue with 3 million severe intoxications reported annually and more than 200,000 deaths, primarily suicides[1–4]. OPs are potent inhibitors of cholinesterases, including acetylcholinesterase (AChE), whose blockade causes a massive accumulation of acetylcholine and overstimulation of cholinergic receptors (ChRs) at both neuromuscular junctions and CNS cholinergic synapses[5]. In the brain, ChR hyperactivation causes epileptic seizures, which if not rapidly treated, may develop into life-threatening *status epilepticus* (SE)[6]. Besides their immediate toxicity, OPs also cause long-term neurological comorbidities, such as psychomotor deficits and recurrent seizures[7,8]. Existing countermeasures combine ChR agonist atropine with an AChE reactivator such as 2-PAM, often associated with γ-aminobutyric acid receptor (GABAR) agonist diazepam (DZP). These treatments are lifesaving, but do not reverse brain damage or prevent subsequent occurrence of seizures

[1]NeuroDiderot, Inserm, Université de Paris, 75019 Paris, France. [2]Département de toxicologie et risques chimiques, Institut de Recherche Biomédicale des Armées (IRBA), 91 220 Brétigny-sur-Orge, France. [3]Institut de Recherche Biomédicale des Armées (IRBA), Unité de Développements Analytiques et Bioanalyse, 91 220 Brétigny-sur-Orge, France. [4]These authors contributed equally: Alexandre Brenet and Julie Somkhit. [5]These authors jointly supervised this work: Nina Dupuis and Nadia Soussi-Yanicostas. ✉email: nadia.soussi@inserm.fr

or psychomotor deficits, emphasizing the need for new, more potent antidotes. To meet this need, an animal model of OP poisoning that would faithfully reproduce the consequences of OP intoxication in humans and be amenable to drug screening would help achieve a better understanding of the pathophysiology of OP poisoning and identify therapeutic entities counteracting the harmful effects of these compounds. Although it has long been known that acute OP intoxication causes neuropathological changes in the brain[8–11], the precise nature of these changes and their extent remain under-researched.

Here, we describe a zebrafish model of OP poisoning and characterize the neuron defects induced by acute intoxication. Over the past decade, besides its rapidly expanding use as a human disease model[12–16], the zebrafish has become one of the leading animal models for toxicology research and drug discovery[17]. The zebrafish is a versatile, powerful and easy-to-breed vertebrate model that offers significant advantages for in vivo drug screening and neurotoxicology investigations. These advantages include a CNS that displays an overall organization similar to that of mammals with full conservation of the different neuronal and glial cell types and all neurotransmitters[18–22]. To model OP poisoning in zebrafish, we chose DFP, an OP analogue of the warfare agent sarin, but less volatile and much less dangerous, that has been widely used as a prototypic OP in toxicology research. In particular, previous studies in rodents have shown that acute DFP poisoning causes potent AChE inhibition, inducing epileptic seizures, neuronal death, memory impairment and neuroinflammation[9,23].

To better understand the physiopathology of OP poisoning and subsequent neuronal deficits, we combined behavioral analysis and in vivo recording of neuronal calcium transients with molecular and immunocytochemical approaches. Our data showed that zebrafish larvae exposed to DFP displayed major inhibition of AChE activity correlated with reduced motor activity. DFP poisoning also induced CNS hyperexcitation as shown by both the large increase in the number of calcium transients in brain neurons and the overexpression of the immediate early genes (IEGs) *fosab, junBa, npas4b,* and *atf3,* transcription factor encoding genes which are transcribed to high levels in the very first hours that follow neuron excitation and epileptic seizures[24,25]. In addition to epileptiform seizures, DFP exposure also caused an increased neuronal apoptosis, both partially mitigated by diazepam administration, suggesting that the increased neuronal apoptosis was a direct consequence of neuronal hyperexcitation. Last, DFP poisoning caused increased NR2B-NMDA subunit receptor accumulation combined with decreased accumulation of both GAD65/67 and gephyrin proteins, suggesting that DFP exposure promotes epileptiform neuronal hyperexcitation as a result of a shift in the glutamatergic/GABAergic balance activity toward glutamate-mediated excitation.

The zebrafish model of DFP poisoning faithfully reproduces the neuronal deficits observed in both humans and rodents exposed to DFP, and also provides interesting new insights into the neurotoxicity of OP agents, making it a promising tool to identify novel, more potent antidotes.

Results

Larvae exposed to DFP showed increased mortality, reduced motility and AChE inhibition. In order to study DFP toxicity, 5 days post-fertilization (dpf) larvae were exposed to DFP and several classic features of OP poisoning were assessed (Fig. 1a). First, we determined DFP toxicity in zebrafish, by exposing 5 dpf larvae to increasing concentrations of DFP (15, 20, 30 and 50 µM) and recording larval survival over a 6 h period. Results showed that all larvae exposed to either 30 µM or 50 µM died during the 6 h incubation period and displayed major morphological defects, such as curved tails and shorter body length, whereas 50% of those exposed to 20 µM died and showed mild morphological defects (Fig. 1b and Supplementary Fig. 1). As we aimed at investigating brain damage associated with mid-acute DFP toxicity, we selected the concentration of 15 µM, which causes a larval lethality of 20% (LC20) and no visible phenotypic defects in surviving larvae. We also checked that DFP was not hydrolyzed during the 6 h incubation time and results showed that DFP diluted in fish water (FW) was almost stable with an average loss of 2% per hour, approximately (Fig. 1c). Then, we analyzed the phenotype of larvae exposed to 15 µM DFP for 6 h and we observed no phenotypic defects in surviving larvae (Fig. 1d–h), except a slight reduction of body length (Fig. 1i). Histopathological analysis also indicated that following a 6 h exposure to 15 µM DFP, surviving larvae did not show any visible histological abnormalities in the brain (Supplementary Fig. 2).

As AChE inhibition is the key hallmark of OP poisoning, we next measured AChE activity in larvae exposed to 15 µM DFP, and we observed a 50% decrease in AChE activity as early as 2 h after DFP addition, worsening to 25% residual activity from 4 h exposure onwards (Fig. 1j). We next investigated whether the decreased AChE activity was correlated with the paralysis of the larvae. Results showed that DFP-treated larvae displayed a markedly decreased locomotor activity compared to control larvae as early as 2 h after DFP addition, as indicated by the distance traveled by larvae, which was recorded using a Zebrabox (ViewPoint) automated device (Fig. 1k). Thus, after DFP exposure, zebrafish larvae displayed reduced motor activity as the likely result of a massive AChE inhibition.

DFP exposure induced neuronal hyperexcitation. Increased transcription of the IEG *c-Fos* in brain neurons has been repeatedly observed following epileptic seizures[26]. As a first investigation of the consequences of DFP poisoning on neuronal activity, we therefore studied, by immunocytochemistry, the accumulation of the Fosab protein, the zebrafish orthologue of c-Fos, in the brain of DFP-treated and control larvae (Fig. 2a,b). Results clearly indicated that DFP-treated larvae displayed a highly significant increase in the number of neurons expressing Fosab ($p < 0.0001$) in both the optic tectum (Fig. 2c–e), and telencephalon (Supplementary Fig. 3). To further investigate whether DFP exposure induces overexpression of other IEGs, we analyzed, by qRT-PCR, the expression in the brain of *fosab*, *atf3*, *junBa*, *npas4a*, and *npas4b*, the zebrafish orthologues of *C-FOS*, *JUNB*, *ATF3*, and *NPAS4*, respectively, four genes that are expressed at high levels in the very first hours that follow epileptic seizures in pharmacological models of epilepsy in rats[25]. Interestingly, qRT-PCR showed a significant

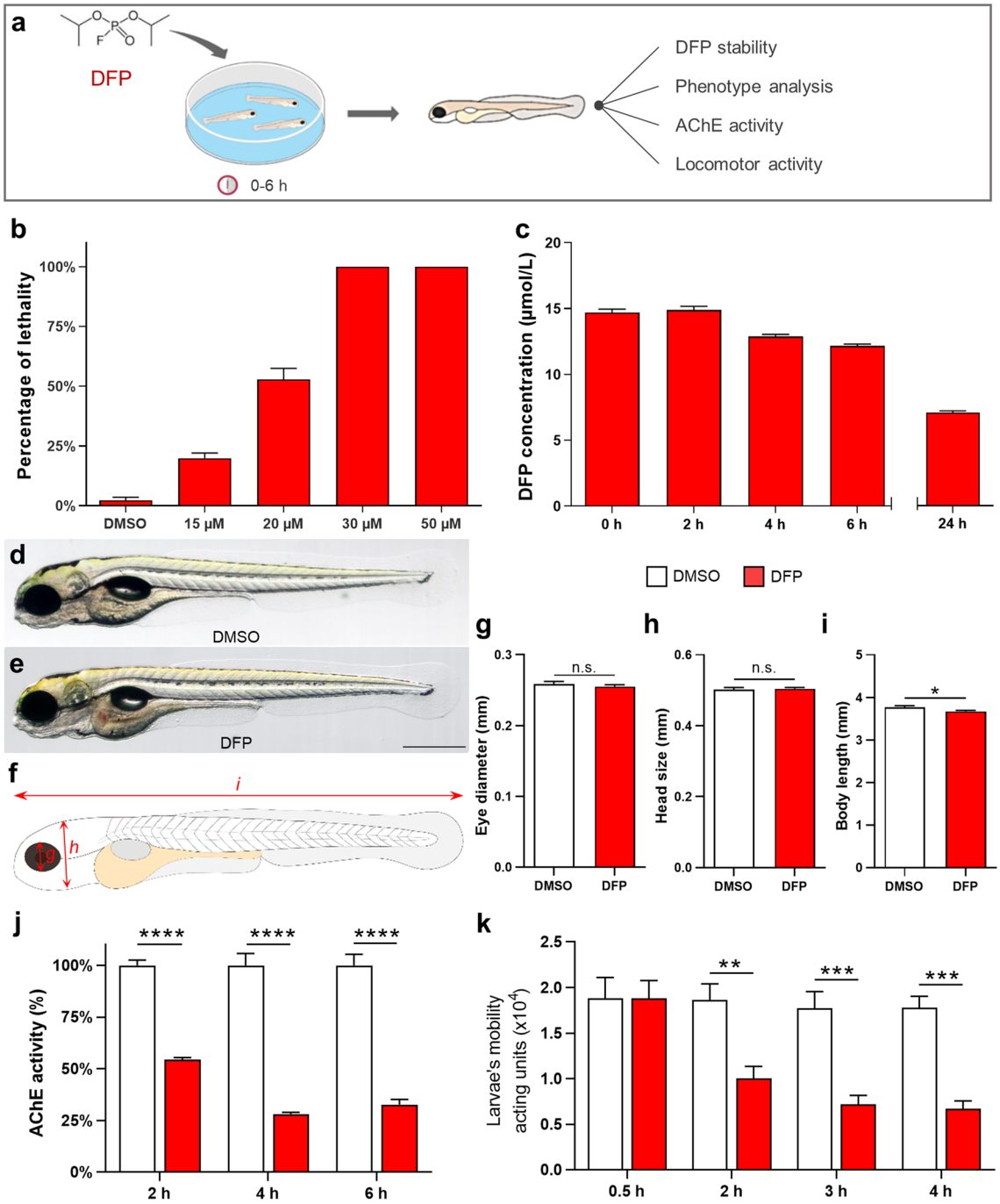

Figure 1. DFP-exposed zebrafish larvae displayed reduced motility and AChE inhibition. (**a**) As experimental set-up, 5 dpf larvae were exposed to 15, 20, 30 or 50 µM DFP or vehicle (1% DMSO) and larval lethality, phenotypic defects, motor activity, and AChE activity were studied during the next 6 h. (**b**) Lethality rates of 5 dpf larvae exposed for 6 h to 15, 20, 30 or 50 µM DFP and selection of 15 µM DFP as optimal concentration (LC20). (**c**) Residual concentrations of DFP measured at different time points from a 15 µM solution diluted in fish water (E3 medium). (**d**,**e**) Morphology of 5 dpf larvae exposed for 6 h to either vehicle (**d**) or 15 µM DFP (**e**). (**f**) Scheme depicting measurements of zebrafish larva morphology. (**g**–**i**) Quantification of eye diameter (**g**), head size (**h**) and body length (**i**) in larvae exposed for 6 h to either vehicle ($n = 26$) or 15 µM DFP ($n = 26$) (Student's unpaired *t*-test: n.s., non-significant; *, $p < 0.05$). (**j**) Quantification of AChE activity in larvae exposed to 15 µM DFP ($n = 5$) or vehicle ($n = 5$), for 2, 4, and 6 h (two-way ANOVA with Sidak's multiple comparisons test: ****, $p < 0.0001$). (**k**) Motor activity of 5 dpf larvae exposed to either 15 µM DFP ($n = 44$) or vehicle ($n = 12$) (two-way ANOVA with Sidak's multiple comparisons test: **, $p < 0.01$; ***, $p < 0.001$).

increase in the accumulation of *fosab* (control: 0.989 ± 0.088 vs. DFP: 5.305 ± 0.804; $p < 0.0001$), *junBa* (control:

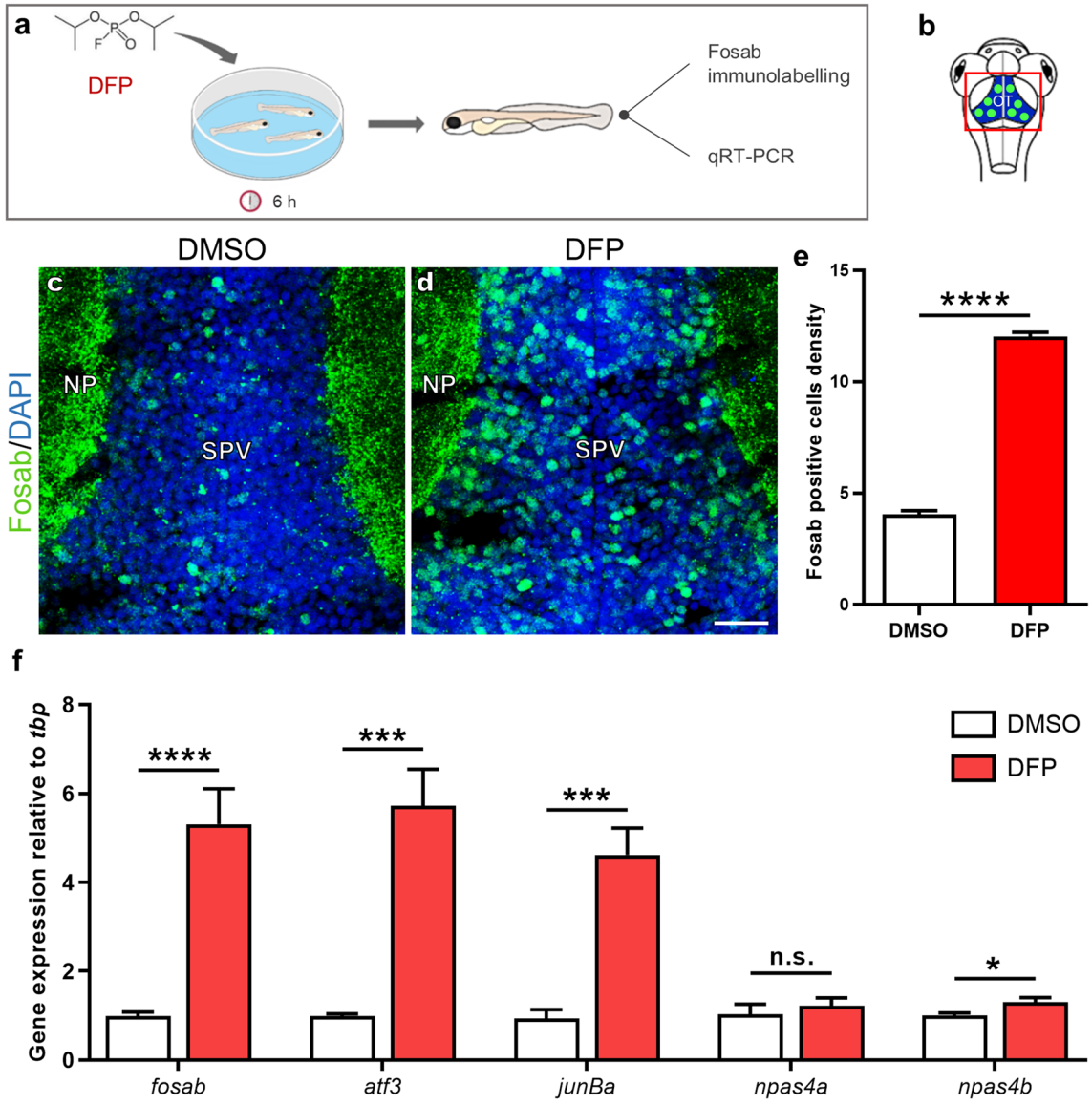

Figure 2. DFP exposure induces overexpression of the IEGs *fosab*, *atf3*, *junBa*, and *npas4b*. (**a**) As experimental set-up, 5 dpf larvae were exposed for 6 h to either 15 µM DFP or vehicle (1% DMSO) before processing for either Fosab immunostaining or brain dissection followed by RNA extraction and qRT-PCR analysis. (**b**) Scheme of a 5 dpf larva head with the red box showing the region of interest in the brain, uncovering the optic tectum (OT). (**c**,**d**) Fosab immunolabeling of optic tectum neurons in 5 dpf larvae exposed to either vehicle (**c**) or 15 µM DFP (**d**). Scale bar: 20 µm. (**e**) Quantification of Fosab-expressing neuron density in the optic tectum of 5 dpf larvae exposed to either vehicle ($N=3$; $n=8$) or 15 µM DFP ($N=3$; $n=11$) (unpaired *t*-test: ****, $p<0.0001$). (**f**) qRT-PCR analysis of the accumulation of *fosab*, *atf3*, *junBa*, *npas4a* and *npas4b* RNAs relative to that of *tbp* in 5 dpf larvae exposed to either vehicle ($n=6$) or 15 µM DFP ($n=6$) (Student's unpaired *t*-test: n.s., non-significant; *, $p<0.05$; ***, $p<0.001$; ****, $p<0.0001$). N = number of larvae and n = number of slices. Abbreviations: NP, neuropil; SPV, stratum periventriculare.

0.938 ± 0.197 vs. DFP: 4.619 ± 0.603; $p<0.001$), *atf3* (control: 0.993 ± 0.047 vs. DFP: 5.723 ± 0.603; $p<0.003$), and *npas4b* (control: 1.007 ± 0.054 vs. DFP: 1.294 ± 0.109; $p<0.05$), in larvae exposed to DFP when compared to that observed in controls (Fig. 2f), suggesting that DFP exposure causes neuronal hyperexcitation. Note that expression of the second zebrafish orthologue of *NPAS4*, *npas4a*, did not change following DFP exposure (control: 1.03 ± 0.228 vs. DFP: 1.226 ± 1.175; $p=0.5$) (Fig. 2f).

We then sought to visualize the increased neuronal activity in larvae exposed to DFP using calcium imaging (Fig. 3a,b), a technique that fully reflects neuronal activity in zebrafish epilepsy models in vivo[14,27]. Five dpf larvae from the transgenic line Tg[Huc:GCaMP5G] were treated with DFP or vehicle (DMSO) and calcium transients were recorded during the following 6 h using time-lapse confocal microscopy (Supplementary Videos 1 and 2). Interestingly, in DFP-treated larvae, we observed numerous intense calcium transients, from approximately 1 h post-exposure onward, which were highly reminiscent of those seen in zebrafish genetic epilepsy models[14].

Moreover, these calcium transients were mostly seen in the neuropil region, where a large number of synaptic connections occur (Fig. 3c–f). Quantification of calcium fluorescence signals confirmed that as early as 1 h after DFP addition, massive calcium transients were detected in DFP-treated larvae (Fig. 3g). We also observed a significant increase in the frequency of the calcium transients from 2 h post-exposure onward (Fig. 3h). Importantly, 3 h after DFP exposure, all larvae displayed numerous massive calcium transients, which were never observed in control larvae, strongly suggesting that zebrafish larvae exposed to acute DFP poisoning display massive neuronal hyperexcitation reminiscent of epileptic seizures. Diazepam (DZP), a GABA receptor agonist of the benzodiazepine family and a component of existing OP cocktail antidotes[28], is a well-known inhibitor of neuronal excitation. We therefore checked whether administration of DZP was able to mitigate the increased number and intensity of calcium transients seen in DFP-exposed larvae. Data showed that massive calcium transients seen in larvae exposed for 5 h to 15 µM DFP were markedly reduced in the minutes that followed the addition of 40 µM DZP (Fig. 3i,j), suggesting that the zebrafish DFP model faithfully reproduces the physiopathology of OP poisoning in humans.

DFP exposure induces increased cell apoptosis. Exposure to warfare OP nerve agents, such as soman, sarin, or VX, causes massive neuronal loss in both humans and animal models[29–33]. We therefore examined whether DFP exposure also caused increased cell death, using both in vivo acridine orange (AO) staining, a vital marker that labels fragmented DNA during late apoptosis stages, and immunodetection of activated-caspase-3 (Act-casp3), a marker of mid-early apoptosis stages (Fig. 4a,b). Interestingly, DFP-exposed larvae displayed a significantly increased number of neurons expressing Act-casp3 compared to that observed in controls (Fig. 4c–e). In addition, in vivo AO labeling confirmed that DFP exposure caused an increased cell apoptosis (Fig. 4f–i). We then investigated whether the increased number of apoptotic cells seen in DFP-treated larvae was a direct consequence of neuronal hyperexcitation. To this end, 5 dpf larvae were co-treated for 6 h with 15 µM DFP and 40 µM DZP, and cell apoptosis was visualized by AO labeling. Results indicate that DZP was able to partially alleviate DFP-induced cell apoptosis (Fig. 4h,i), strongly suggesting a link between neuronal hyperexcitation and cell death.

Increased NR2B-NMDA subunit receptor expression and decreased GAD65/67 and gephyrin protein accumulation in DFP exposed larvae. It has been shown that following OP exposure, neuronal seizures are associated with both an increased glutamatergic response and excessive NMDA receptor activation[34–36]. To examine whether accumulation of the NR2B-NMDA subunit receptor, a component of the main excitatory glutamate receptor, was modified following DFP exposure, brain sections of larvae exposed to DFP or controls were analyzed by immunocytochemistry using an anti-NR2B-NMDA antibody (Fig. 5a,b). Interestingly, results showed a clear increase in the accumulation of NR2B-NMDA protein in the tectal neuropil of DFP-exposed larvae, compared to that seen in controls (Fig. 5c,d). Moreover, the DFP-induced increased NR2B-NMDA accumulation at excitatory synapses was confirmed by quantification of synaptic puncta in the tectal neuropil (Fig. 5e). We also analyzed the synaptic protein gephyrin, which is a scaffolding protein expressed at the inhibitory post-synaptic terminals (Fig. 5a,f). Quantification of this labeling showed a marked decrease in gephyrin synaptic puncta density in the tectal neuropil in DFP-exposed larvae compared to controls (Fig. 5g–i). In contrast no NR2B-NMDA or gephyrin immunolabeling were observed in cell bodies of the stratum periventricular (Supplementary Fig. 4). To further characterize brain reorganization induced by DFP exposure, we analyzed, by immunohistochemistry, the accumulation of glutamate decarboxylase 65/67 (GAD65/67), the enzymes involved in GABA synthesis, the main inhibitory transmitter (Fig. 5a,j). Interestingly, quantification of immunolabeling signals indicated that DFP-treated larvae displayed markedly decreased accumulation of GAD65/67 proteins (Fig. 5k–m). Altogether, these results strongly suggest that DFP exposure induces neuronal hyperexcitation as a result of simultaneous increased glutamatergic activity and decreased GABAergic signaling.

Discussion

Because of the widespread use of organophosphorus (OP) compounds for agricultural purposes and the lack of fully effective countermeasures, OP poisoning remains a major public health issue worldwide, with several million intoxications and over 200,000 deaths reported each year[37,38], emphasizing the need for fully efficient antidotes to alleviate OP toxicity. To help fill this gap, we used the possibilities offered by zebrafish larvae and developed a vertebrate model of OP poisoning to investigate the consequences of OP exposure on neuronal functions and neuronal network activity. As an OP compound, we chose DFP, a moderately toxic compound previously used for OP toxicology research[39]. In good agreement with the results gained with rodent OP poisoning models[6,40], zebrafish larvae exposed to DFP displayed marked AChE inhibition and muscle paralysis, two important hallmarks of OP poisoning. More importantly, unlike rodent OP intoxication models, in which premature death due to respiratory failure must imperatively be prevented by the simultaneous addition of low dose atropine and oximes, there is no need to treat DFP-exposed zebrafish with acetylcholine modulators, making DFP-exposed zebrafish larvae an accurate animal model to investigate the physiopathology of OP poisoning. In particular, as a pure OP poisoning model, zebrafish larvae also offer a powerful tool to test the effects of anti-convulsive agents or other OP antidotes, in the absence of either muscarinic antagonists or cholinesterase reactivators.

Previous results in both humans and rodent models have shown that acute OP poisoning causes neuronal hyperexcitation leading to epileptic seizures[6]. In good agreement with this observation, we first observed that zebrafish larvae exposed to DFP displayed a considerably increased accumulation of the Fosab protein in brain neurons. *c-Fos* is a member of the IEG family, widely used as a molecular marker of neuronal activity, and overexpressed in a large number of animal epilepsy models[41–43], suggesting that acute DFP exposure causes

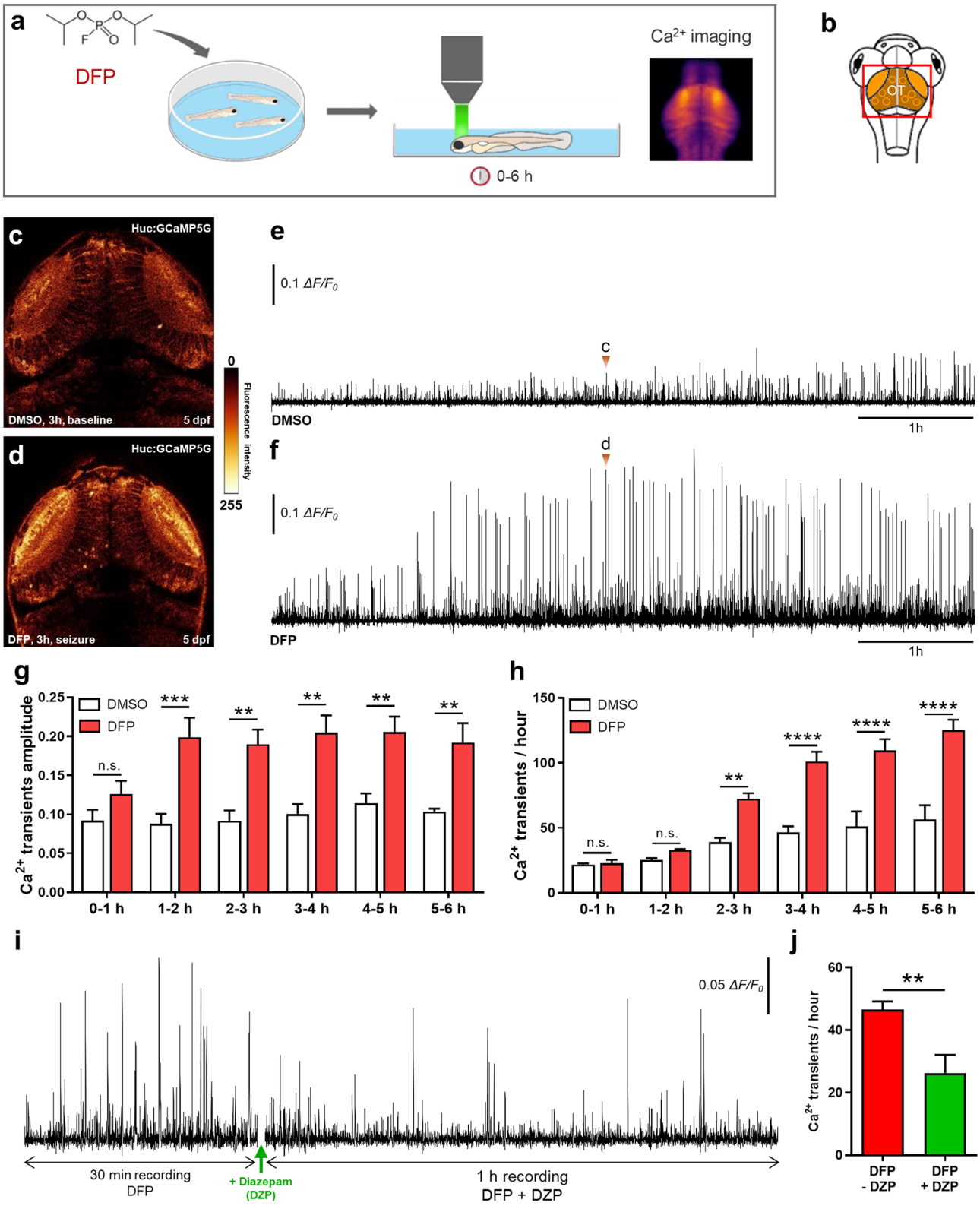

neuronal hyperexcitation. Using qRT-PCR analysis we next showed that DFP exposure also induced a massive accumulation of transcripts of the IEGs *fosab, atf3, junBa,* and *npas4b,* providing another indication that DFP induces a massive neuronal hyperexcitation in zebrafish larvae. To further investigate whether DFP exposure causes neuronal hyperexcitation, we used calcium imaging, a recent technology that enables the visualization of neuronal excitation and epileptic seizures in living zebrafish larvae[14,27,44]. Interestingly, in larvae exposed to acute DFP poisoning, we observed a massive increase in the number of neuronal calcium transients compared to those seen in controls, and also a significant increase in the amplitude of the transients in DFP-treated larvae.

◂**Figure 3.** DFP exposure caused neuronal hyperexcitation. (**a**) As experimental set-up, 5 dpf Tg[Huc:GCaMP5G] larvae were exposed to either 15 µM DFP or vehicle (1% DMSO), and calcium transients were recorded in brain neurons during the next 6 h. (**b**) Scheme of a 5 dpf larva head with the red box showing the region of interest in the brain, uncovering the optic tectum (OT). (**c**,**d**) Snapshot views of calcium imaging in a 5 dpf Tg[Huc:GCaMP5G] larva brain showing baseline calcium transients (**c** in Fig. 2e) and seizure-like hyperactivity seen 3 h after exposure to 15 µM DFP (**d** in Fig. 2f). (**e**,**f**) Baseline calcium transients detected in 5 dpf Tg[Huc:GCaMP5G] control larvae ($n=3$) (**e**) and massive calcium transients detected in 5 dpf Tg[Huc:GCaMP5G] larvae exposed for 6 h to 15 µM DFP ($n=4$) (**f**). (**g**) Amplitude of calcium transients detected in 5 dpf Tg[Huc:GCaMP5G] larvae at different time points following exposure to either 15 µM DFP ($n=4$) or vehicle ($n=3$) (two-way ANOVA with Sidak's multiple comparisons test: n.s., non-significant; **, $p<0.01$; ***, $p<0.001$). (**h**) Number of calcium transients showing $\Delta F/F_0>0.04$ in 5 dpf Tg[Huc:GCaMP5G] larvae at different time points following exposure to either 15 µM DFP ($n=4$) or vehicle ($n=3$) (two-way ANOVA with Sidak's multiple comparisons test: n.s., non-significant; **, $p<0.01$; ****, $p<0.0001$). (**i**) Pattern of calcium transients seen in 5 dpf Tg[Huc:GCaMP5G] larvae exposed for 5 h to 15 µM DFP and then to 15 µM DFP + 40 µM diazepam (DZP) for an additional hour. (**j**) Number of calcium transients showing $\Delta F/F_0>0.04$ in 5 dpf Tg[Huc:GCaMP5G] larvae exposed for 5 h to 15 µM DFP and then to 15 µM DFP + 40 µM diazepam (DZP) for an additional hour ($n=6$) (Student's unpaired t-test: **, $p<0.01$).

Last, these calcium transients detected in brain neurons of DFP-exposed larvae were significantly diminished after addition of diazepam, a GABA receptor agonist. Altogether, these observations demonstrate that after acute DFP poisoning, zebrafish larvae display epileptiform neuronal hyperexcitation. In humans suffering from acute OP intoxication, whenever neuronal hyperexcitation is not rapidly treated, epileptic seizures eventually develop into SE, a major life-threatening neurological condition[6,45], which also causes long-term brain damage[46,47]. Interestingly, in the zebrafish model of OP poisoning presented here, we observed that almost all the larvae displayed numerous massive calcium transients from 2 to 3 h after DFP exposure onward, which were strongly reminiscent of those associated with generalized seizures seen in both genetic and pharmacological zebrafish epilepsy models[14,27]. Altogether, these findings strongly suggest that DFP exposure causes epileptiform neuronal hyperexcitation in zebrafish larvae, eventually leading to a status epilepticus-like condition. This validated DFP model could be used to identify novel OP antidotes, and especially neuroprotective entities preventing the long-lasting neuronal morbidities associated with OP exposure. In particular, new AChE reactivators or other efficient countermeasures could be identified on the basis of their ability to restore locomotor activity or counteract epileptogenic effects of OP poisoning.

Together with AChE inhibition and epileptic seizures, massive neuronal death is another hallmark of OP poisoning[23] also observed in DFP-exposed zebrafish larvae, as demonstrated by acridine orange staining and Act-casp3 immunocytochemistry, two markers of late and mid-early apoptosis stages, respectively. Importantly, given that the number of Act-casp3 positive cells was approximately doubled only 6 h after OP addition, and that the cleavage of Pro-Caspase 3 into Act-casp3 is a mid-early stage event in the intrinsic apoptotic cascade, these data suggest that DFP-induced neuronal apoptosis is initiated in the very first hours that follow OP poisoning, a time frame also matching the massive calcium transients seen in DFP-treated individuals. Altogether, these results suggest that the increased rate of neuronal apoptosis seen in DFP-treated individuals was a consequence of glutamate excitotoxicity due to epileptiform neuronal hyperexcitation. Alterations in proteolytic cleavage of pro-caspase 1 and 3 have already been described in different experimental epilepsy models[48,49]. However, the relationship between neuronal excitation, glutamate excitotoxicity and neuronal apoptosis remains poorly understood. At the cellular level, it has long been known that epileptiform neuronal hyperexcitation relies on massive glutamate releases, inducing glutamate receptor over-activation at glutamatergic excitatory synapses[34–36]. In the case of OP poisoning, it has been shown that acute OP intoxication induces activation of NMDA receptors[50], which in turn causes neuronal seizures and apoptosis[46,51]. Interestingly, in the model of OP poisoning presented here, hyperexcitation of brain neurons was correlated with both increased accumulation of the NR2B subunit of excitatory NMDA receptor and decreased accumulation of gephyrin and GAD65/67 proteins, two important components of GABAergic inhibitory signaling. These results suggest that after DFP poisoning, neuronal hyperexcitation is due to a shift in the glutamatergic/GABAergic activity balance of brain neurons toward excitatory states.

We report here on a zebrafish model of OP poisoning that faithfully recapitulates the neuronal deficits observed in humans, including AChE inhibition, epileptiform neuronal hyperexcitation, and neuronal apoptosis. Moreover, this vertebrate model does not require the simultaneous addition of acetylcholine modulators, unlike rodent models of OP poisoning, thus providing a pure and accurate model for large-scale in vivo screening of entities that could restore CNS functions after OP poisoning and alleviate the long-term neurological sequelae of such intoxication.

Materials and methods

Fish husbandry and zebrafish lines. Zebrafish were kept at 26–28 °C in a 14 h light/10 h dark cycle. Embryos were collected by natural spawning and raised in E3 solution at 28.5 °C. To inhibit embryo pigmentation, 0.003% 1-phenyl-2-thiourea was added at 1-day post-fertilization (dpf). Wild-type AB fish was originally purchased from the Zebrafish International Resource Center (Eugene, OR, USA) and Tg[HuC:GCaMP5G] transgenic line[52] was a gift from Dr. George Debrégeas (Laboratoire Jean Perrin, Paris). These lines were raised in our facility. All animal experiments were conducted at the French National Institute of Health and Medical Research (Inserm) UMR 1141 in Paris in accordance with European Union guidelines for the handling of laboratory animals (https://ec.europa.eu/environment/chemicals/lab_animals/home_en.htm), and were approved by

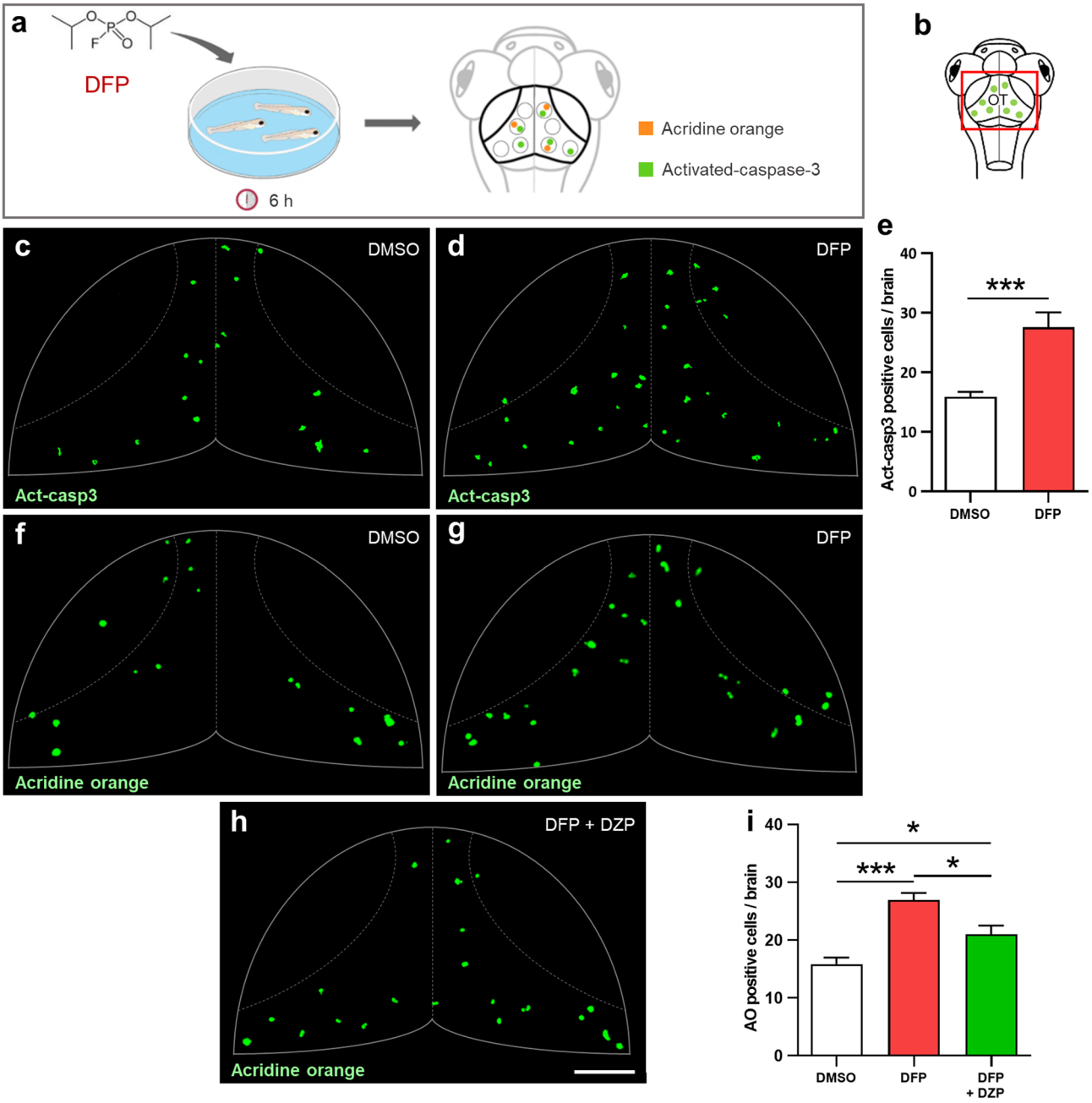

Figure 4. DFP exposure increased cell apoptosis. (**a**) As experimental set-up, 5 dpf larvae were exposed to either 15 µM DFP or vehicle (1% DMSO) for 6 h, before processing for either acridine orange (AO) staining or anti-activated caspase-3 (Act-casp3) immunolabeling. (**b**) Scheme of a 5 dpf larva head with the red box showing the region of interest in the brain, uncovering the optic tectum (OT). (**c**,**d**) Act-casp3 immunolabeling of OT neurons in 5 dpf larvae exposed for 6 h to either vehicle (**c**) or 15 µM DFP (**d**). (**e**) Quantification of Act-casp3-positive neurons in 5 dpf larvae exposed for 6 h to either 15 µM DFP ($n = 12$) or vehicle ($n = 12$) (Student's unpaired t-test with Welch's correction: ***, $p < 0.001$). (**f**–**h**) Visualization of AO-labeled apoptotic neurons in 5 dpf larvae exposed for 6 h to either vehicle (**f**), or 15 µM DFP (**g**) or 15 µM DFP + 40 µM diazepam (**h**). (**i**) Quantification of the number of acridine orange positive cells in 5 dpf larvae exposed for 6 h to either vehicle ($n = 24$), or 15 µM DFP ($n = 17$) or 15 µM DFP + 40 µM diazepam (DZP) ($n = 10$) (one-way ANOVA with Tukey's multiple comparisons test: *, $p < 0.05$; ***, $p < 0.001$). Scale bar: 50 µm.

the Direction Départementale de la Protection des Populations de Paris and the French Animal Ethics Committee under reference No. 2012-15/676-0069.

DFP treatment. Diisopropylfluorophosphate (DFP) was purchased from Sigma Aldrich. A stock solution (5.46 mM), stored at − 20 °C, was diluted extemporaneously to 15 µM in 1% DMSO/E3 medium. Control zebrafish larvae were treated with 1% DMSO/E3 medium.

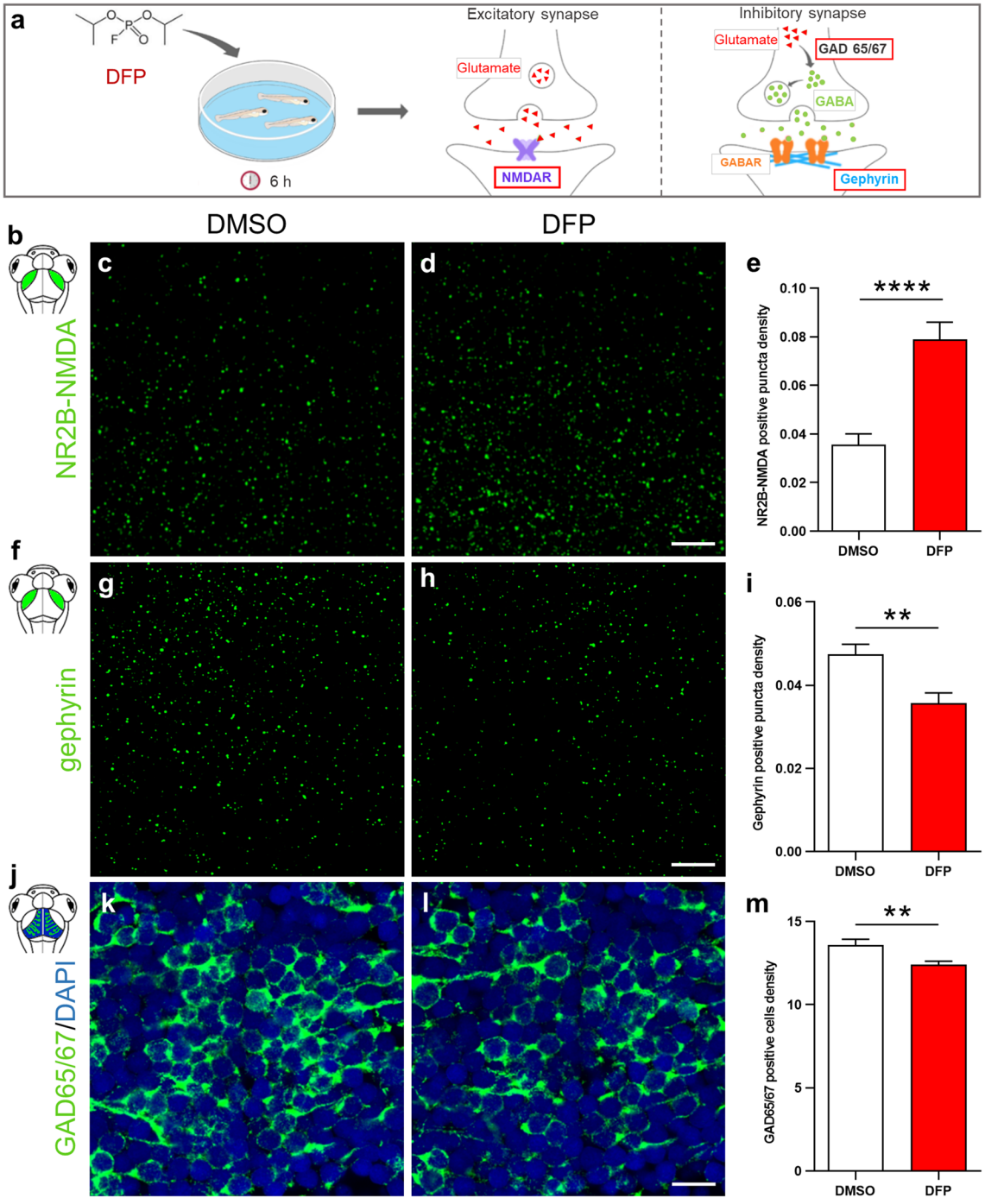

Figure 5. DFP exposure caused increased NR2B-NMDA subunit receptor accumulation combined with decreased gephyrin and GABA signaling. (**a**) As experimental set-up, 5 dpf larvae were exposed to either 15 µM DFP or vehicle (DMSO) for 6 h, prior to being processed for NR2B-NMDA, gephyrin or GAD 65/67 immunolabeling. (**b**) Scheme of 5 dpf larva head highlighting the tectal neuropils in green. (**c**,**d**) NR2B-NMDA receptor immunolabelling of 5 dpf larvae brains exposed to either DMSO (**c**) or 15 µM DFP (**d**). Scale bar: 5 µm. (**e**) Quantification of NR2B-NMDA puncta density in 5 dpf larvae treated for 6 h with either DMSO ($N=4$; $n=22$) or 15 µM DFP ($N=4$; $n=26$) (Mann Whitney : ****, $p<0.0001$). (**f**) Scheme of 5 dpf larva head highlighting the tectal neuropils in green. (**g**,**h**) Gephyrin immunolabelling of 5 dpf larvae brains exposed to either DMSO (**g**) or 15 µM DFP (**h**). Scale bar: 5 µm. (**i**) Quantification of gephyrin puncta density in 5 dpf larvae treated for 6 h with either DMSO ($N=4$; $n=18$) or 15 µM DFP ($N=4$; $n=18$) (Student unpaired *t*-test: **, $p<0.01$). (**j**) Scheme of 5 dpf larva head highlighting stratum periventriculare in blue and green. (**k**,**l**) GAD65/67 immunolabelling of neurons in the optic tectum of 5 dpf larvae brains exposed to either DMSO (**k**) or 15 µM DFP (**l**). Scale bar :10 µm. (**m**) Quantification of the density of neurons expressing GAD65/67 protein in the optic tectum of 5 dpf larvae exposed to either DMSO ($N=4$; $n=18$) or 15 µM DFP ($N=4$; $n=19$) (Student unpaired *t*-test : **, $p<0.01$). N = number of larvae and n = number of slices.

Measurement of DFP stability (see supplementary Materials & Methods).

Morphological analysis. Five dpf larvae were anesthetized and lateral views of the whole body were acquired using a Zeiss Stereomicroscope at the same magnification. Body length, eye size, and head size were then measured using ImageJ 1.52p (https://imagej.nih.gov/ij/). Body length was measured from the anterior tip of the body to the caudal peduncle. Eye size and brain surface area were measured by specifying the eye and brain boundaries.

Hematoxylin/eosin staining (see supplementary Materials & Methods).

Measurement of AChE activity (see supplementary Materials & Methods).

Zebrafish larval locomotor activity. Larvae locomotor activity was measured, as previously described[14], using a Zebrabox (View Point), an automated infrared tracking device, with ZebraLab 5.13.0.240 software (https://www.viewpoint.fr/en/home). Five dpf larvae were individually dispatched in a 96-well plate in approximately 200 µl of E3 medium containing either 1% DMSO or 15 µM DFP. The plate was then placed in the recording chamber for a 30-min habituation in the dark and in silence. Locomotor activity was then recorded for 4 h using the following settings: animal color was set to black and threshold detection to 12. The locomotion activity was quantified as the sum of all pixels showing intensity changes during the recording time and plotted as "acting units".

qRT-PCR. For RNA isolation, larvae were homogenized using a syringe equipped with a 26G needle (7 larvae per sample) using the RNA XS Plus kit (Qiagen, Hilden, Germany). cDNAs were synthesized using the iScript cDNA Synthesis Kit (Bio-Rad, Munich, Germany) and qPCR was performed using iQ SYBR Green Supermix (Bio-Rad). Samples were run in triplicate. Expression levels were normalized to that of the *tbp* gene. The primers (Eurofins Genomics, Ebersberg, Germany) used are listed in Supplementary Table 1.

Neuronal calcium transient imaging. Calcium activity was recorded and quantified as previously described in Brenet et al. (2019)[14]. Five dpf larvae were paralyzed using 300 µM pancuronium bromide (PB) and embedded in 1.3% low-melting agarose in the center of a 35 mm glass-bottomed dish, and then covered with 3 mL of E3 solution containing 300 µM PB. The recording chamber was then placed under a Leica SP8 laser scanning confocal microscope equipped with a 20×/0.75 multi-immersion objective. Vehicle (1% DMSO) or DFP (15 µM) was added to the E3 medium and calcium activity was recorded for 6 h. Calcium fluorescent signals were recorded on a single focal plan, located approximately in the middle of the optic tectum, at a 512 × 512-pixel image resolution and a frame rate of 2 images per second. Fluorescence intensity of each frame was measured using a homemade macro on ImageJ 1.52p (https://imagej.nih.gov/ij/). Fluorescence variations ($\Delta F/F_0$) were calculated using Microsoft Excel (for Windows 2013, version 15.0.4569.1506) by subtracting the mean fluorescence intensity of all frames (F_0) and dividing the results by F_0. A subtraction of the mean value of the lowest (all values under the median) within a 20 s sliding window around the point was finally applied to correct the fluorescence drift occurring during long calcium recordings. Fluorescence variations greater than 0.04 $\Delta F/F_0$ were considered as calcium events upon visual confirmation since the detection system may detect false events.

Diazepam treatment. 5 dpf Tg[Huc:GCaMP5G] larvae were exposed to 15 µM DFP for 5 h, PB-paralyzed and embedded in 1.1% low-melting agarose in the center of a 35 mm glass-bottomed dish, and then covered with an E3 solution containing 15 µM DFP and 300 µM PB. Calcium transients were first monitored for 30 min. Diazepam (40 µM DZP, Sigma) was then added and calcium transients were recorded for an additional hour. Visualization and recording of calcium transients were carried out as described above.

Acridine orange labeling of apoptotic cells. To quantify neuronal cell death, we used in vivo acridine orange (AO) staining of fragmented DNA molecules in apoptotic cells. Five dpf larvae treated with either vehicle or DFP were incubated for 30 min in AO (1/2000, VectaCell), thoroughly washed several times, PB-paralyzed and agar-embedded. 120 µm stacks of brain sections were then acquired using a Leica SP8 laser scanning confocal microscope equipped with a 20×/0.75 multi-immersion objective. In addition to AO staining, brains were stained with anti-activated-caspase-3 and processed as previously described[14] (see supplementary Materials & Methods).

Immunohistochemistry (see also Supplementary Table 2 for details on antibodies used). For protein immunodetection, zebrafish larvae were fixed in 4% formaldehyde, incubated overnight in 15% sucrose at 4 °C, embedded in 7.5% gelatin/15% sucrose solution, flash frozen in isopentane at −45 °C and stored at −80 °C until use. For gephyrin immunodetection, unfixed larvae were directly incubated for 30 min in 15% sucrose at room temperature and then embedded in 7.5% gelatin/15% sucrose solution, flash frozen in isopentane at −45 °C and stored at −80 °C until use. Frozen embedded larvae were cut into 20 µm cryostat sections. For Fosab staining, we strictly applied the protocol described by Chatterjee et al. (2015)[53]. For anti-GAD56/67 and anti-gephyrin immunolabeling, we used the endogenous biotin blocking procedure (Avidin/Biotin Blocking Kit, Dako, code No. X0590) according to the manufacturer's instructions. Sections were then blocked and permeabilized with 0.2% gelatine, 0.25% Triton X100 diluted in 1X PBS for 1 h at room temperature and then incubated overnight at room temperature with either anti-GAD65/67 (1:300) or anti-gephyrin (1:100). After several washes, GAD65/67 and gephyrin proteins were detected using biotinylated goat anti-rabbit and streptavidine Alexa 488 (Molecular Probes; catalog No. S32355; used at 1:400 dilution). Sections were counterstained for

10 min with 0.1% DAPI (Sigma, St. Louis, MO). For anti-NMDA-NR2B, immunohistochemistry was performed as previously described[54]. Briefly, brain tissue sections were blocked and permeabilized with 0.2% gelatin, 0.25% Triton X100 diluted in PBS for 1 h at room temperature and then incubated overnight at room temperature with anti-NMDA-NR2B antibody (1:300). After several washes, sections were incubated for 1 h with anti-rabbit coupled to Alexa Fluor 488. Sections were counterstained for 10 min with DAPI (Sigma-Aldrich, used at 1:3000) before mounting.

Quantification of NR2B and gephyrin puncta labeling. Sections stained with anti-NR2B-NMDA and anti-gephyrin antibodies were imaged at full resolution (voxel size: 0.063 × 0.063 × 0.3 µm) using a Leica SP8 laser scanning confocal microscope equipped with a 63 × /1.4 oil-immersion objective. Images were then processed with AutoQuant X3.1 software (https://www.mediacy.com/autoquantx3) and the density of NR2B or gephyrin labeled puncta was quantified using a homemade ImageJ macro (Zsolt Csaba, Inserm UMR1141). After stacking all images, a median filter was applied, a threshold on the fluorescence intensity was then set to select NR2B-NMDA or gephyrin puncta. Puncta were identified as accumulation of more than two pixels (0.126 µm) in diameter, which lead to an average punctum size of 0.34 µm. The density of NR2B-NMDA or gephyrin puncta were calculated by dividing the number of labeled puncta detected in the tectal neuropil by the surface area of this region.

Quantification of Fosab- and GAD65/67-positive neuron density. Sections hybridized with anti-Fosab and anti-GAD65/67 antibodies were imaged using a Leica SP8 laser scanning confocal microscope equipped with a 40×/1.3 oil-immersion objective. The neurons expressing Fosab or GAD65/67 were manually counted with ImageJ 1.52p (https://imagej.nih.gov/ij/) on sections of optic tectum or telencephalon. The number of positive neurons was then divided by the surface area of the corresponding regions to calculate a density of neurons expressing those proteins in larvae exposed to DFP or vehicle.

Statistical analysis. Statistical analyses were performed using GraphPad Prism 8.4.3.686 (https://www.graphpad.com/scientific-software/prism/). Data were first challenged for normality using the Shapiro–Wilk test. Data with a normal distribution were analyzed by a two-tailed unpaired *t*-test. Data not showing normal distribution were analyzed using a two-tailed Mann–Whitney test. All graphs show mean ± s.e.m.

Data availability

The datasets generated during the current study are available from the corresponding author on reasonable request.

Received: 5 March 2020; Accepted: 19 October 2020
Published online: 05 November 2020

References

1. Mew, E. J. *et al.* The global burden of fatal self-poisoning with pesticides 2006–15: systematic review. *J. Affect. Disord.* **219**, 93–104 (2017).
2. Konickx, L. A. *et al.* Reactivation of plasma butyrylcholinesterase by pralidoxime chloride in patients poisoned by WHO class II toxicity organophosphorus insecticides. *Toxicol. Sci.* https://doi.org/10.1093/toxsci/kft217 (2013).
3. Pereira, E. F. R. *et al.* Animal models that best reproduce the clinical manifestations of human intoxication with organophosphorus compounds. *J. Pharmacol. Exp. Ther.* **350**, 313–321 (2014).
4. Jett, D. A. Neurological aspects of chemical terrorism. *Ann. Neurol.* **61**, 9–13 (2007).
5. Lotti, M. Clinical toxicology of anticholinesterase agents in humans. In *Hayes' Handbook of Pesticide Toxicology* (ed. Krieger, R.) 1543–1589 (Elsevier, Amsterdam, 2010). https://doi.org/10.1016/B978-0-12-374367-1.00072-0.
6. Todorovic, M. S., Cowan, M. L., Balint, C. A., Sun, C. & Kapur, J. Characterization of status epilepticus induced by two organophosphates in rats. *Epilepsy Res.* **101**, 268–276 (2012).
7. Chen, Y. Organophosphate-induced brain damage: mechanisms, neuropsychiatric and neurological consequences, and potential therapeutic strategies. *Neurotoxicology* **33**, 391–400 (2012).
8. Collombet, J.-M. Nerve agent intoxication: recent neuropathophysiological findings and subsequent impact on medical management prospects. *Toxicol. Appl. Pharmacol.* https://doi.org/10.1016/j.taap.2011.07.003 (2011).
9. Li, Y. *et al.* Spatiotemporal pattern of neuronal injury induced by DFP in rats: a model for delayed neuronal cell death following acute OP intoxication. *Toxicol. Appl. Pharmacol.* **253**, 261–269 (2011).
10. McDonough, J. H. & Shih, T. M. Neuropharmacological mechanisms of nerve agent-induced seizure and neuropathology. *Neurosci. Biobehav. Rev.* **21**, 559–579 (1997).
11. Yamasue, H. *et al.* Human brain structural change related to acute single exposure to sarin. *Ann. Neurol.* **61**, 37–46 (2007).
12. Yanicostas, C., Ernest, S., Dayraud, C., Petit, C. & Soussi-Yanicostas, N. Essential requirement for zebrafish anosmin-1a in the migration of the posterior lateral line primordium. *Dev. Biol.* **320**, 469–479 (2008).
13. Martin, E. *et al.* Spatacsin and spastizin act in the same pathway required for proper spinal motor neuron axon outgrowth in zebrafish. *Neurobiol. Dis.* **48**, 299–308 (2012).
14. Brenet, A., Hassan-Abdi, R., Somkhit, J., Yanicostas, C. & Soussi-Yanicostas, N. Defective excitatory/inhibitory synaptic balance and increased neuron apoptosis in a zebrafish model of dravet syndrome. *Cells* **8**, 1199 (2019).
15. Ghoumid, J. *et al.* ZEB2 zinc-finger missense mutations lead to hypomorphic alleles and a mild Mowat-Wilson syndrome. *Hum. Mol. Genet.* **22**, 2652–2661 (2013).
16. Yanicostas, C. *et al.* Requirement for Zebrafish ataxin-7 in differentiation of photoreceptors and cerebellar neurons. *PLoS ONE* **7**, e50705 (2012).
17. MacRae, C. A. & Peterson, R. T. Zebrafish as tools for drug discovery. *Nat. Rev. Drug Discov.* **14**, 721–731 (2015).
18. Lessman, C. A. The developing zebrafish (*Danio rerio*): a vertebrate model for high-throughput screening of chemical libraries. *Birth Defects Res. Part C Embryo Today Rev.* **93**, 268–280 (2011).
19. Delvecchio, C., Tiefenbach, J. & Krause, H. M. The Zebrafish: a powerful platform for in vivo, HTS drug discovery. *Assay Drug Dev. Technol.* **9**, 354–361 (2011).

20. Rinkwitz, S., Mourrain, P. & Becker, T. S. Zebrafish: An integrative system for neurogenomics and neurosciences. *Prog. Neurobiol.* **93**, 231–243 (2011).
21. Ito, H. & Yamamoto, N. Non-laminar cerebral cortex in teleost fishes?. *Biol. Lett.* **5**, 117–121 (2009).
22. Wullimann, M. F. Secondary neurogenesis and telencephalic organization in zebrafish and mice: a brief review. *Integr. Zool.* **4**, 123–133 (2009).
23. Flannery, B. M. *et al.* Persistent neuroinflammation and cognitive impairment in a rat model of acute diisopropylfluorophosphate intoxication. *J. Neuroinflammation* **13**, 1–16 (2016).
24. Dragunow, M., Yamada, N., Bilkey, D. K. & Lawlor, P. Induction of immediate-early gene proteins in dentate granule cells and somatostatin interneurons after hippocampal seizures. *Mol. Brain Res.* **13**, 119–126 (1992).
25. Lösing, P. *et al.* SRF modulates seizure occurrence, activity induced gene transcription and hippocampal circuit reorganization in the mouse pilocarpine epilepsy model. *Mol. Brain* **10**, 1–22 (2017).
26. Szyndler, J. *et al.* Mapping of c-Fos expression in the rat brain during the evolution of pentylenetetrazol-kindled seizures. *Epilepsy Behav.* **16**, 216–224 (2009).
27. Liu, J. & Baraban, S. C. Network properties revealed during multi-scale calcium imaging of seizure activity in zebrafish. *eNeuro* **6**, ENEURO.0041-19.2019 (2019).
28. Verrotti, A., Milioni, M. & Zaccara, G. Safety and efficacy of diazepam autoinjector for the management of epilepsy. *Exp. Rev. Neurother.* **15**, 127–133 (2014).
29. Petras, J. M. Neurology and neuropathology of soman-induced brain injury: an overview. *J. Exp. Anal. Behav.* **61**, 319–329 (1994).
30. Shih, T.-M., Duniho, S. M. & Mcdonough, J. H. Control of nerve agent-induced seizures is critical for neuroprotection and survival. *Toxicol. Appl. Pharmacol.* https://doi.org/10.1016/S0041-008X(03)00019-X (2003).
31. Kim, Y. B. *et al.* Organophosphate-induced brain injuries: delayed apoptosis mediated by nitric oxide. *Environ. Toxicol. Pharmacol.* **7**, 147–152 (1999).
32. Kaur, P., Radotra, B., Minz, R. W. & Gill, K. D. Impaired mitochondrial energy metabolism and neuronal apoptotic cell death after chronic dichlorvos (OP) exposure in rat brain. *Neurotoxicology* **28**, 1208–1219 (2007).
33. Gunay, N. *et al.* Protective effects of Y-27632 on acute dichlorvos poisoning in rats. *Am. J. Emerg. Med.* **28**, 268–274 (2010).
34. Lallement, G. *et al.* Involvement of the different rat hippocampal glutamatergic receptors in development of seizures induced by soman: an autoradiographic study. *Neurotoxicology* **12**, 655–664 (1991).
35. Lallement, G. *et al.* Involvement of glutamatergic system of amygdala in generalized seizures induced by soman: comparison with the hippocampus. *C. R. Acad. Sci. III* **313**, 421–426 (1991).
36. Lallement, G. *et al.* Effects of soman-induced seizures on different extracellular amino acid levels and on glutamate uptake in rat hippocampus. *Brain Res.* **563**, 234–240 (1991).
37. Dawson, A. H. *et al.* Acute human lethal toxicity of agricultural pesticides: a prospective cohort study. *PLoS Med.* **7**, e1000357 (2010).
38. Bertolote, J. M., Fleischmann, A., Eddleston, M. & Gunnell, D. Deaths from pesticide poisoning: a global response. *Br. J. Psychiatry* **189**, 201–203 (2006).
39. Saunders, B. *Some Aspects of the Chemistry and Toxic Action of Organic Compounds Containing Phosphorus and Fluorine* (Cambridge University Press Wiley, New York, 1957).
40. McCarren, H. S. & McDonough, J. H. Anticonvulsant discovery through animal models of status epilepticus induced by organophosphorus nerve agents and pesticides. *Ann. N. Y. Acad. Sci.* **1374**, 144–150 (2016).
41. Dragunow, M. & Robertson, H. A. Kindling stimulation induces c-fos protein(s) in granule cells of the rat dentate gyrus. *Nature* **329**, 441–442 (1987).
42. Le Gal, G. & Salle, L. Long-lasting and sequential increase of c-fos oncoprotein expression in kainic acid-induced status epilepticus. *Neurosci. Lett.* **88**, 127–130 (1988).
43. Simler, S. *et al.* C-fos expression after single and kindled audiogenic seizures in Wistar rats. *Neurosci. Lett.* **175**, 58–62 (1994).
44. Diaz Verdugo, C. *et al.* Glia-neuron interactions underlie state transitions to generalized seizures. *Nat. Commun.* **10**, 1–13 (2019).
45. Trinka, E. *et al.* A definition and classification of status epilepticus—report of the ILAE task force on classification of status epilepticus. *Epilepsia* **56**, 1515–1523 (2015).
46. Shih, T. M. & McDonough, J. H. Neurochemical mechanisms in soman-induced seizures. *J. Appl. Toxicol.* **17**, 255–264 (1997).
47. Tryphonas, L. & Clement, J. G. Histomorphogenesis of soman-induced encephalocardiomyopathy in Sprague-Dawley rats. *Toxicol. Pathol.* **23**, 393–409 (1995).
48. Henshall, D. C., Chen, J. & Simon, R. P. Involvement of caspase-3-like protease in the mechanism of cell death following focally evoked limbic seizures. *J. Neurochem.* **74**, 1215–1223 (2000).
49. Narkilahti, S., Pirttila, T. J., Lukasiuk, K., Tuunanen, J. & Pitkanen, A. Expression and activation of caspase 3 following status epilepticus in the rat. *Eur. J. Neurosci.* **18**, 1486–1496 (2003).
50. Kaur, S., Singh, S., Chahal, K. S. & Prakash, A. Potential pharmacological strategies for the improved treatment of organophosphate-induced neurotoxicity. *Can. J. Physiol. Pharmacol.* **92**, 893–911 (2014).
51. Solberg, Y. & Belkin, M. The role of excitotoxicity in organophosphorous nerve agents central poisoning. *Trends Pharmacol. Sci.* **18**, 183–185 (1997).
52. Akerboom, J. *et al.* Optimization of a GCaMP calcium indicator for neural activity imaging. *J. Neurosci.* https://doi.org/10.1523/JNEUROSCI.2601-12.2012 (2012).
53. Chatterjee, D., Tran, S., Shams, S. & Gerlai, R. A simple method for immunohistochemical staining of zebrafish brain sections for c-fos protein expression. *Zebrafish* **12**, 414–420 (2015).
54. Puverel, S., Nakatani, H., Parras, C. & Soussi-Yanicostas, N. Prokineticin receptor 2 expression identifies migrating neuroblasts and their subventricular zone transient-amplifying progenitors in adult mice. *J. Comp. Neurol.* **512**, 232–242 (2009).

Author contributions

A.B. and J.S. performed the experiments, the analysis, and designed the figures. R.H.A., A.I., D.S., C.R., O.B. and N.T. helped carry out the experiments. N.D. helped supervise the project. C.Y., G.D.B., F.N. and N.D. contributed to the final manuscript. N.S.Y. supervised the project and wrote the manuscript.

Competing interests

The authors declare no competing interests.

Additional information

Supplementary information is available for this paper at https://doi.org/10.1038/s41598-020-76056-8.

Correspondence and requests for materials should be addressed to N.S.-Y.

Reprints and permissions information is available at www.nature.com/reprints.